A mouse model of stenosis distal to an arteriovenous fistula recapitulates human central venous stenosis

Ryosuke Taniguchi, MD, PhD,[a,b] Shun Ono, MD,[a,c] Toshihiko Isaji, MD, PhD,[a,b] Jolanta Gorecka, MD,[a] Shin-Rong Lee, MD, PhD,[a] Yutaka Matsubara, MD, PhD,[a,d] Bogdan Yatsula, PhD,[a] Jun Koizumi, MD, PhD,[c] Toshiya Nishibe, MD, PhD,[e] Katsuyuki Hoshina, MD, PhD,[b] *and* Alan Dardik, MD, PhD,[a,f,g] *New Haven, and West Haven, Conn; and Tokyo, Kanagawa, and Fukuoka, Japan*

ABSTRACT

Objective: Central venous stenosis (CVS) is a major cause of arteriovenous fistula (AVF) failure. However, central veins are relatively inaccessible to study with conventional Doppler ultrasound methods. To understand mechanisms underlying AVF failure owing to CVS, an animal model was established that creates a stenosis distal to an AVF. We hypothesized that this mouse model will show comparable morphology and physiology to human CVS.

Methods: An aortocaval fistula was created between the distal aorta and inferior vena cava (IVC); a stenosis was then created distal to the fistula by partial IVC ligation. Sham-operated animals, AVF without venous stenosis, and venous stenosis without AVF were used as controls. Physiologic properties of the IVC, both upstream and downstream of the stenosis, or the corresponding sites in models without stenosis, were assessed with ultrasound examination on days 0 to 21. The spectral broadening index was measured to assess the degree of disturbed shear stress. The IVC was harvested at day 21 and specimens were analyzed with immunofluorescence.

Results: The IVC diameter of mice with an AVF and stenosis showed increased upstream ($P = .013$), but decreased downstream diameter ($P = .001$) compared with mice with an AVF but without a stenosis, at all postoperative times (days 3-21). IVC wall thickness increased in mice with an AVF, compared with IVC without an AVF (upstream of stenosis: 13.9 μm vs 11.0 μm vs 4.5 μm vs 3.9 μm; $P = .020$; downstream of stenosis: 6.0 μm vs 6.6 μm vs μm 4.5 μm vs 3.8 μm; $P = .002$; AVF with stenosis, AVF, stenosis, sham, respectively). AVF patency significantly decreased in mice with an AVF and stenosis by day 21 (50% vs 90%; $P = .048$). The IVC of mice with AVF and stenosis showed a venous waveform with pulsatility as well as enhanced velocity at and downstream of the stenosis; similar waveforms were observed in a human case of CVS. Downstream to the stenosis, the spectral broadening index was significantly higher compared with mice with AVF alone (1.06 vs 0.78; $P = .011$; day 21), and there was a trend towards less immunoreactivity of both Krüppel-like factor 2 and phosphorylated-endothelial nitric oxide synthase compared with mice with an AVF alone.

Conclusions: Partial IVC ligation distal to a mouse aortocaval fistula alters the fistula diameter and wall thickness, decreases patency, and increases distal disturbed flow compared with fistulae without a distal stenosis. Our mouse model of stenosis distal to an AVF may be a faithful representation of human CVS that shows similar morphology and physiology, including disturbed shear stress. (JVS—Vascular Science 2020;1:109-22.)

Clinical Relevance: A mouse model of venous stenosis distal to an arteriovenous fistula shows similar Doppler waveforms as those observed in a human case of central venous stenosis. These mice retain disturbed shear stress in the vein distal to the fistula, characterized by a sustained increase of the spectral broadening index and diminished expression of proteins upregulated by laminar shear stress. This novel mouse model will enable investigation of the physiology and downstream molecular pathways involved in central venous stenosis in humans.

Keywords: Arteriovenous fistula; Central venous stenosis; Shear stress; Disturbed flow; Spectral broadening index

The prevalence of patients with end-stage renal disease in the United States continues to increase, with approximately 750,000 cases in 2017, resulting in $35.9 billion in Medicare costs.[1] Arteriovenous fistulae (AVF) are the gold standard for hemodialysis access, secondary to their superior patency, reduced infection rate, and improved long-term survival, compared with arteriovenous grafts or central venous catheters.[2-4] Nonetheless, nearly

From the Vascular Biology and Therapeutics Program, Yale School of Medicine, New Haven[a]; the Division of Vascular Surgery, The University of Tokyo, Bunkyo-ku, Tokyo[b]; the Department of Diagnostic Radiology, Tokai University School of Medicine, Isehara, Kanagawa[c]; the Department of Surgery and Sciences, Kyushu University, Fukuoka[d]; the Department of Cardiovascular Surgery, Tokyo Medical University, Shinjuku-ku, Tokyo[e]; the Division of Vascular and Endovascular Surgery, Department of Surgery, Yale School of Medicine, New Haven[f]; and the Department of Surgery, VA Connecticut Healthcare Systems, West Haven.[g]

Author conflict of interest: none.

Correspondence: Alan Dardik, MD, PhD, Department of Surgery, Yale School of Medicine, 10 Amistad St, Rm 437, PO Box 208089, New Haven, CT 06520-8089 (e-mail: alan.dardik@yale.edu).

The editors and reviewers of this article have no relevant financial relationships to disclose per the JVS-Vascular Science policy that requires reviewers to decline review of any manuscript for which they may have a conflict of interest.

2666-3503

https://doi.org/10.1016/j.jvssci.2020.07.003

one-half of AVF fail within 6 months after surgery, requiring a better understanding of the basic mechanisms underlying AVF failure.[5] Although juxta-anastomotic stenosis is an important cause of early failure to mature, stenosis in the venous outflow of the fistula, including the central veins, is a major cause of AVF failure.[6,7] Because central venous stenosis (CVS) is relatively inaccessible to study using conventional ultrasound examination, CVS remains challenging to detect and mechanisms of CVS formation remain poorly understood.

Animal models of CVS could help to determine the physiologic and molecular changes distal to an AVF that lead to CVS formation as well as access failure; however, there are currently few such models. Although large animal models have vessel diameters that more closely approximate human vessels, murine models allow for genetic and pharmacologic manipulation, as well as higher throughput. We have previously established a mouse AVF model that recapitulates human AVF maturation and early failure, with early vessel remodeling characterized by wall thickening and vessel dilation by day 21, as well as subsequent failure in one-third of these AVF by day 42 secondary to juxta-anastomotic neointimal hyperplasia.[8] We recently described a technical modification of this model to reproducibly create a stenosis in the inferior vena cava (IVC), effectively creating a central stenosis distal to the AVF.[9]

We have previously used Doppler ultrasound examination to detect differences in both magnitude and frequency of shear stress in the mouse AVF model,[8-10] and changes in shear stress correlate with reduced expression of antiproliferative and anti-inflammatory endothelial genes.[11,12] We hypothesized that our mouse model of CVS distal to an AVF shows similar morphology, physiology, and waveforms compared with human CVS.

ARTICLE HIGHLIGHTS

- **Type of Research:** Basic science research
- **Key Findings:** Mice with partial ligation of the inferior vena cava distal to an arteriovenous fistula showed similar Doppler waveforms as those observed in a human case of central venous stenosis. These mice retained disturbed shear stress in the vein distal to the fistula, characterized by sustained increase of the spectral broadening index and diminished expression of proteins upregulated by laminar shear stress.
- **Take Home Message:** This novel mouse model enables investigation of the physiology and downstream molecular pathways potentially involved in central venous stenosis in humans.

METHODS

Mouse model of CVS in the outflow of an AVF. All animal experiments were performed in strict compliance with federal guidelines and with approval from the Institutional Animal Care and Use Committee of Yale University. Mice used for this study were male, wild-type C57BL6/J; female mice were excluded owing to their different AVF inflow shear stress.[13] Mice were 9 to 12 weeks of age when the surgeries were performed. Briefly, after exposing the IVC and aorta, an 8-0 Nylon suture was placed around the IVC in the mid infrarenal IVC at the place of intended stenosis in the venous outflow from the AVF site in the distal aorta/IVC. An aortocaval fistula was then created by puncturing the distal aorta into the IVC using a 25-G needle, as previously described.[8] The IVC and a 22-G catheter, which is used as a spacer, were then ligated firmly but without deforming the catheter. The spacer was then removed to create a partial ligation and the vessels were unclamped.[9] Perioperative heparin was not used. Visualization of pulsatile arterial blood flow in the IVC was used to assess initial technical success of AVF creation (n = 20; Fig 1, *A*). Sham-operated animals (n = 5), animals with AVF without venous stenosis (n = 10), and animals with venous stenosis without AVF (n = 8) were used as controls. The inflow aorta cranial to the AVF was termed "proximal" to the AVF and the outflow IVC also cranial to the AVF was termed "distal" to the AVF (Fig 1, *A*). Within the IVC distal to the AVF, the segment caudal to the IVC ligation was termed "upstream" of the stenosis and the segment cranial to the IVC ligation was termed "downstream" of the stenosis (Fig 1, *A*).

Ultrasound measurements. Doppler ultrasound examination (Vevo 770 High-Resolution Imaging System; Fujifilm Visual Sonics Inc., Toronto, Canada) with a RMV704 probe (40 MHz) was used to confirm the patency of the AVF; fistulae were considered patent with an increased end-diastolic velocity (EDV) of the inflow aorta and occlusion was confirmed with a diminished EDV (Fig 1, *B*).

Diameter, as well as physiologic properties including peak systolic velocity (PSV), EDV, time-averaged maximum velocity (TAMV) and spectral broadening (Fig 1, *C*) were measured by ultrasound examination. Blood flow, resistance index, and shear stress were calculated from the values obtained by ultrasound (Fig 1, *D*). Blood viscosity was assumed to be constant at 0.035 poise. In mice with an AVF, the spectral broadening index was used to quantify the spectrum of velocity components and defined as the amount of spectral broadening normalized to the maximum velocity (Fig 1, *C* and *D*).[14,15]

Measurements were obtained at the infrarenal aorta, at the point of IVC stenosis, as well as 2 mm upstream and 2 mm downstream of the stenosis (Fig 1, *A*). The corresponding sites were measured in models without a

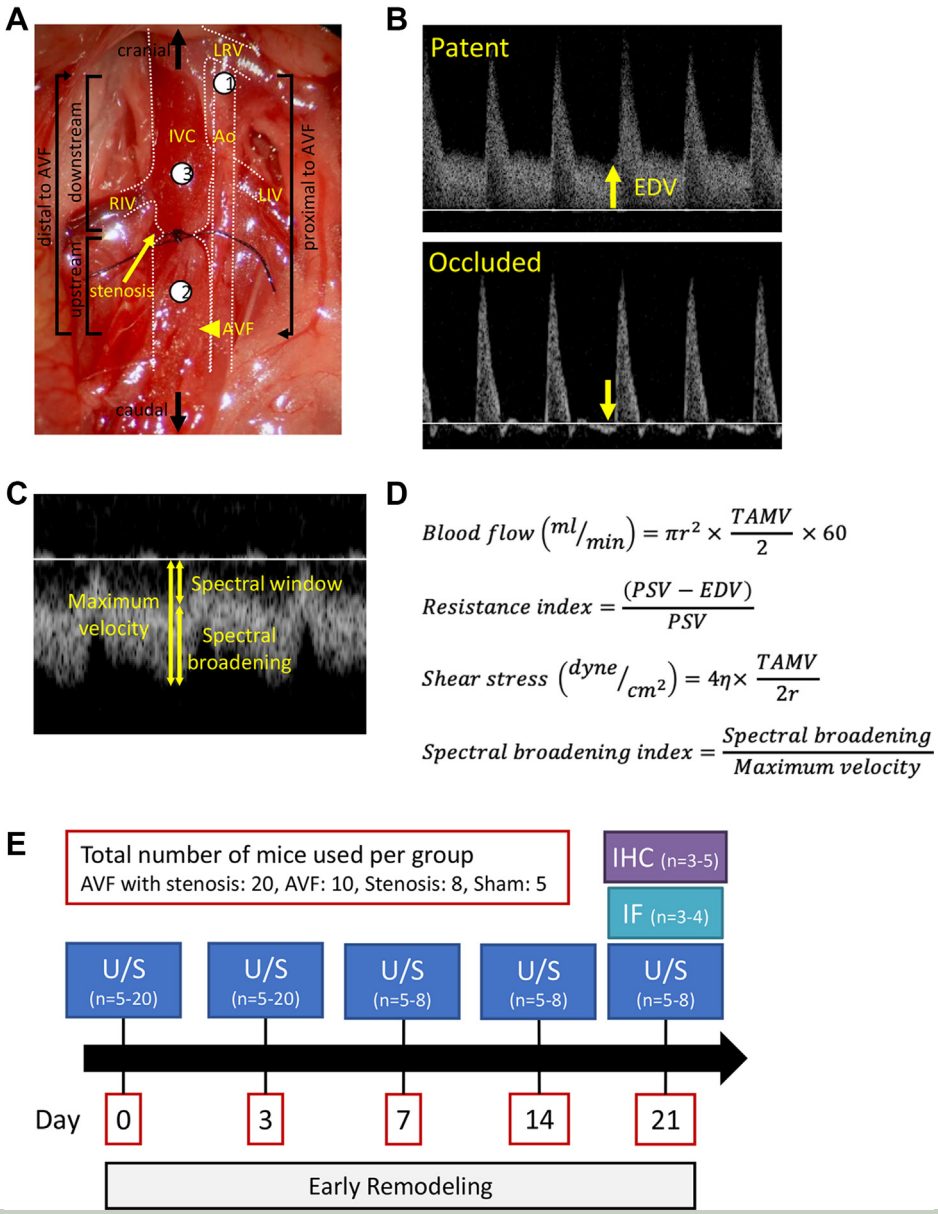

Fig 1. The stenosis model with an arteriovenous fistula (*AVF*). **A,** Representative postprocedural photograph of the mouse stenosis model with an AVF. The aorta and IVC are outlined with interrupted white lines. Numbered circles show the location of where ultrasound measurements were obtained: ①, infrarenal aorta; ②, upstream (2 mm) of the stenosis; ③, downstream (2 mm) of the stenosis. **B,** Representative Doppler waveforms of the mouse infrarenal aorta with a patent AVF (top) and an occluded AVF (bottom). The end-diastolic velocity (*EDV*) is increased in the presence of a patent fistula, whereas the EDV is diminished in the presence of an occluded fistula. **C,** Representative Doppler waveform of the IVC distal to an AVF. The spectral window is the clear black zone between the spectral line and the baseline. Spectral broadening is the widening of the spectral line. Maximum velocity = Spectral window + Spectral broadening. **D,** Calculation formulae for data acquired from ultrasound measurements. Blood viscosity, η, was assumed to be constant at 0.035 poise. **E,** Flow chart showing the experimental design of this study and the number of animals used in each analysis. *Ao,* Aorta; *IF,* immunofluorescence; *IHC,* immunohistochemistry; *IVC,* inferior vena cava; *LIV,* left iliolumbar vein; *LRV,* left renal vein; *PSV,* peak systolic velocity; *r,* radius (in centimeters); *RIV,* right iliolumbar vein; *TAMV,* time-averaged maximum velocity; *U/S,* ultrasound.

stenosis or an AVF. Ultrasound examination was performed before the operation (day 0 values) and serially postoperatively up to day 21.

Histology. Animals were humanely killed and perfused with normal saline followed by 10% formalin via the left ventricle under physiologic pressure and the AVF was extracted en bloc. The tissue was then embedded in paraffin and cut in 5-μm cross-sections. Elastin Van Gieson staining was used to measure the medial thickness of the aorta or the intima-media thickness of the IVC in 5-μm cross-sections of the vessels at the infrarenal aorta, the stenosis of the IVC, 2 mm upstream and 2 mm downstream of the stenosis (Fig 1, *A*). The corresponding sites were analyzed in models without a stenosis or an AVF. Masson's trichrome staining was used to measure the collagen area fractions in 5-μm cross-sections of the IVC, 2 mm upstream of the stenosis. Digital images of the sections were captured with a microscope (BX40; Q Color 5; Olympus America, Center Valley, Pa) and were analyzed using ImageJ software (National Institutes of Health, Bethesda, Md). Four equidistant points of the aortic wall and eight equidistant points of the IVC wall were averaged per cross-section to obtain the mean wall thickness.[8,16] Additional unstained serial cross-sections in the same region were used for immunofluorescence microscopy.

Immunofluorescence. Tissue sections were deparaffined using xylene and rehydrated in a graded series of alcohols. Sections were heated in citric acid buffer (pH 6.0) at 100°C for 10 minutes for antigen retrieval. The sections were then blocked with 2% bovine serum albumin in phosphate-buffered saline (PBS) containing 0.1% Tween20, for 1 hour at room temperature, before incubation overnight at 4°C with the primary antibodies diluted in 2% bovine serum albumin in PBS. Primary antibodies used were anti-vWF (1:400, ab11713; Abcam, Cambridge, Mass), anti-Krüppel-like factor 2 (Klf2, 1:100, LS-B5627, LifeSpan Biosciences, Seattle, Wash), anti-phosphorylated endothelial nitric oxide synthase (p-eNOS, 1:50, 9570; Cell Signaling Technology, Danvers, Mass), anti-α-smooth muscle actin (1:500, 14-9760-82; eBioscience, San Diego, Calif), anti-CD68 (1:100, MCA1957, Bio-Rad, Hercules, Calif), and anti-CD3 (1:20, MAB4841, R&D, Minneapolis, Minn). Sections were then treated with secondary antibodies at room temperature for 1 hour using Alexa Fluor 488- or 568-conjugated IgG (Life Technologies, Eugene, Ore). Sections were stained with Slow Fade Gold Antifade Mount with DAPI (Life Technologies) and a coverslip was applied. Digital fluorescence images were captured and the intensity of the immunoreactive signal was measured using Image J software.

Human percutaneous angioplasty. The principles outlined in the Declaration of Helsinki were followed, and approval of Tokai University was obtained; informed consent was obtained before the intervention. During an elective case of a percutaneous angioplasty to treat CVS in the right proximal subclavian vein in the outflow of an AVF a 0.014-inch guidewire equipped with a Doppler transducer tip (FloWire, Philips, Amsterdam, the Netherlands) was used to obtain Doppler waveforms. Measurements were obtained within the stenosis as well as upstream and downstream to the stenosis.

Experimental design in mice. During the early remodeling phase (days 0-21), including baseline (day 0) immediately before AVF creation, the hemodynamic parameters of interest (diameter, velocity, and flow) were measured in the aorta and the IVC. Immunofluorescence and immunohistochemical analyses were performed at the end of the early remodeling phase (day 21). AVF patency was assessed up to day 21 (Fig 1, *E*).

Statistical analysis. All data were analyzed using Prism 8 software (GraphPad Software, Inc., La Jolla, Calif). Error bars represent the standard error of the mean. The Shapiro-Wilk test was performed to analyze normality and the F test was performed to evaluate homogeneity of variances. For two-group comparisons with normally distributed data, the unpaired Student *t*-test was used to compare data with equal variances among groups and the unpaired Student *t*-test with Welch correction was used to compare data with unequal variances. For multiple group comparisons with normally distributed data, a one-way or two-way analysis of variance followed by the Tukey's post hoc test was used. Patency and survival were analyzed with Kaplan-Meier curves to display the distribution of occlusion and death events, respectively, detected over time. *P* values of less than .05 were considered significant.

RESULTS

Morphology of the mouse aorta and IVC. To establish a novel model of CVS, the IVC of mice was partially ligated distal to an aortocaval AVF (Fig 1, *A*); three groups of control mice were used, including mice with an AVF without a distal stenosis, distal stenosis without an AVF, and neither an AVF nor a stenosis (sham procedure). The diameter of the infrarenal aorta proximal to the AVF site in animals with an AVF and distal stenosis was significantly increased, compared with the diameter of sham-operated animals (Fig 2, *A*; red vs black). Mice with an AVF but without a stenosis showed a similar increase in aortic diameter to that seen in mice with an AVF and a stenosis (Fig 2, *A*; blue vs red). The presence of an IVC stenosis alone had little impact on the diameter of the aorta (Fig 2, *A*; green).

Consistent with previous studies, the diameter of the IVC distal to the AVF site in mice with an AVF but without a stenosis also increased compared with the IVC diameter of sham-operated mice (Fig 2, *B* and *D*; blue vs black), both upstream and downstream of the stenosis.[8,10,17,18]

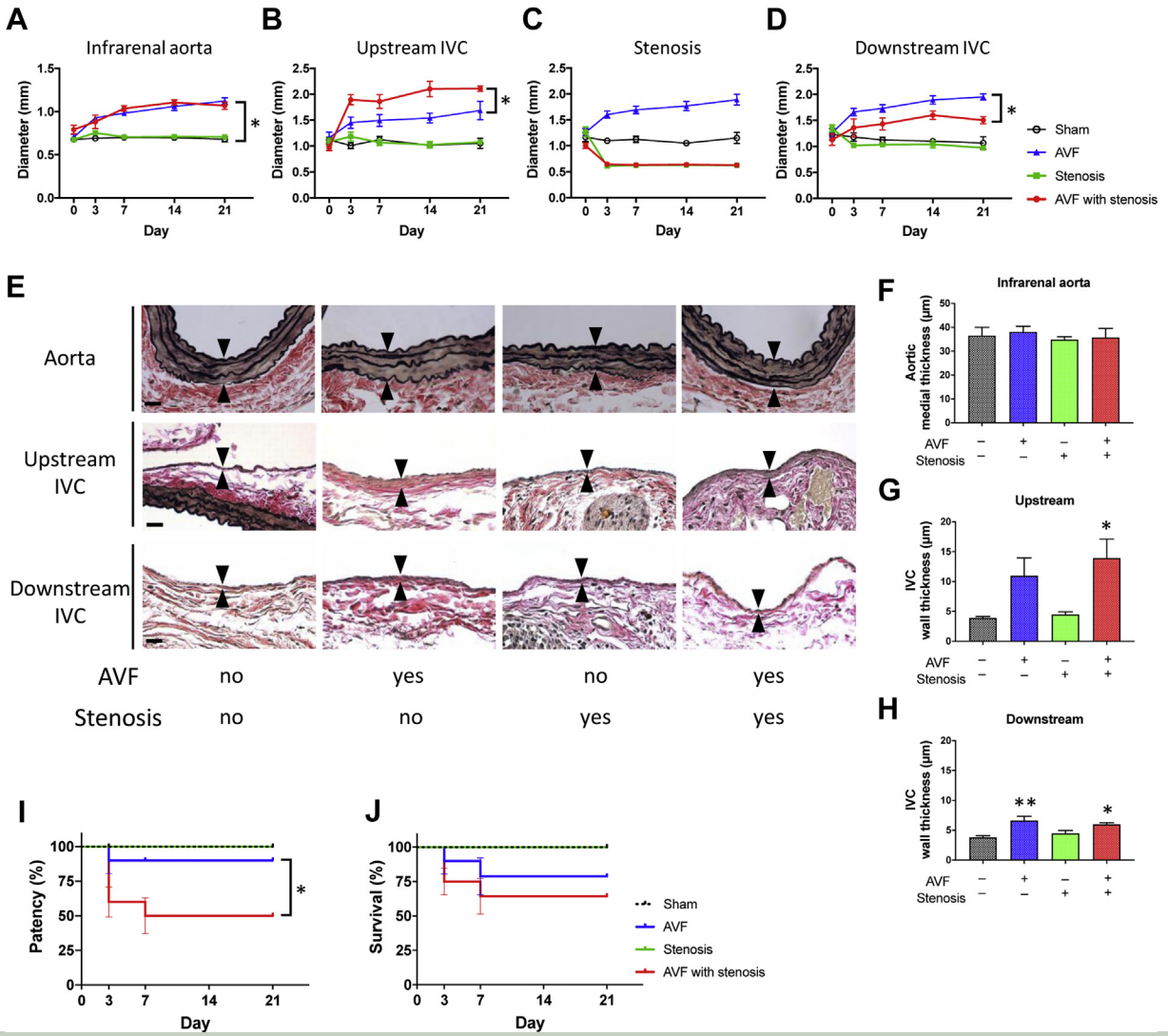

Fig 2. Morphology of the mouse aorta and inferior vena cava (IVC). **A-D,** Line graphs showing diameter of the **(A)** infrarenal aorta ($P < .001$; analysis of variance [ANOVA]). *$P < .0001$ (post hoc, AVF with stenosis vs sham, day 21). **B**, Inferior vena cava (*IVC*), upstream, $P < .0001$ (ANOVA). *$P = .0130$ (post hoc, arteriovenous fistula [*AVF*] with stenosis vs AVF, day 21). **C,** IVC, stenosis ($P < .0001$, ANOVA). **D,** IVC, downstream ($P < .0001$; ANOVA). *$P = .0010$ (post hoc, AVF with stenosis vs AVF, day 21; n = 5-8). **E,** Representative photomicrographs of Van Gieson staining showing wall thickness of the infrarenal aorta (top row) and IVC, upstream (middle row) and downstream (bottom row) of stenosis, at day 21. Scale bar = 20 μm. **F-H,** Bar graphs showing **(F)** aortic medial thickness ($P = .9006$, ANOVA). **G,** IVC upstream wall thickness ($P = .0201$, ANOVA). *$P = .0442$ (post hoc, AVF with stenosis vs sham). **H,** IVC downstream wall thickness ($P = .0024$, ANOVA). *$P = .0160$ (post hoc, AVF with stenosis vs sham). **$P = .0038$ (post hoc, AVF vs sham; n = 4-5). **I,** Line graph showing cumulative patency rate up to day 21 ($P = .0481$, log-rank). AVF with stenosis vs AVF (n = 10-20). **J,** Line graph showing overall survival up to day 21 ($P = .3940$, log-rank). AVF with stenosis vs AVF (n = 10-20).

Mice with both a stenosis and an AVF also showed a large upstream IVC diameter and smaller IVC downstream diameter, compared with mice with an AVF but without a stenosis (Fig 2, *B* and *D*; red vs blue). In mice with an IVC stenosis alone, the IVC diameter was similar to sham-operated mice, both upstream and downstream of the stenosis (Fig 2, *B* and *D*; green vs black). At the site of the stenosis, the IVC diameter of the mice with stenosis alone (green), as well as with stenosis and an AVF (red), was consistently approximately 0.6 mm (Fig 2, *C*); the diameter at the site of the venous ligation was reproducible and consistent throughout the course of study.

Tissue was harvested on postoperative day 21 for assessment of aorta and IVC wall thickness. There were no obvious collateral vessels or lower extremity edema observed in any mice. There were no differences in infrarenal aortic wall thickness among the groups (Fig 2, *E* and *F*). Compared with sham-operated mice,

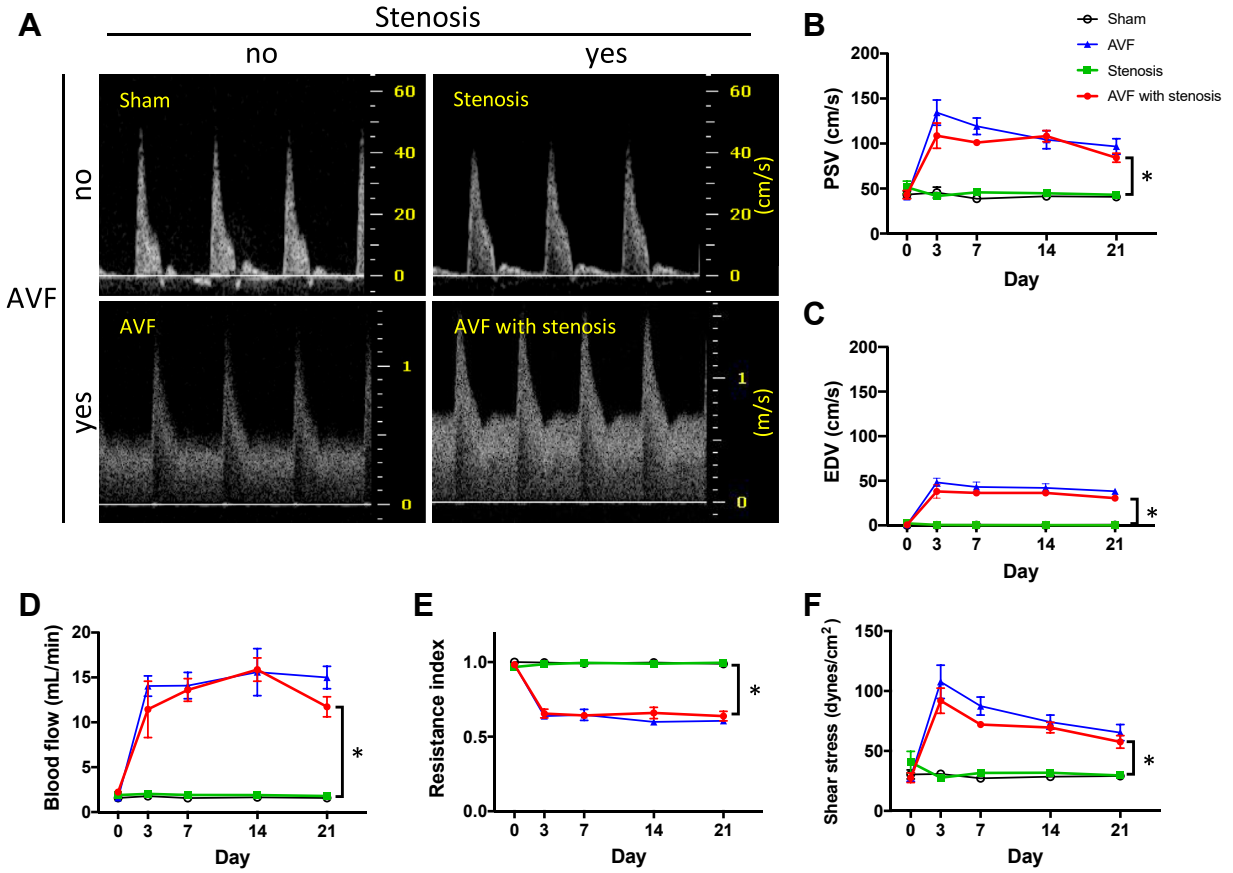

Fig 3. Physiologic properties of the mouse aorta. **A,** Representative Doppler waveforms of the infrarenal aorta at postoperative day 3. **B,** Line graph showing peak systolic velocity (PSV) of the aorta, $P < .0001$ (analysis of variance [ANOVA]). *$P = .0008$ (post hoc, arteriovenous fistula [*AVF*] with stenosis vs sham, day 21; n = 5-8). **C,** Line graph showing end-diastolic velocity (EDV) of the aorta ($P < .0001$, ANOVA). *$P = .0048$ (post hoc, AVF with stenosis vs sham, day 21; n = 5-8). **D,** Line graph showing blood flow of the aorta ($P < .0001$, ANOVA). *$P = .0021$ (post hoc, AVF with stenosis vs sham, day 21; n = 5-8). **E,** Line graph showing resistance index of the aorta ($P < .0001$, ANOVA). *$P = .0010$ (post hoc, AVF with stenosis vs sham, day 21; n = 5-8). **F,** Line graph showing shear stress of the aorta ($P < .0001$, ANOVA). *$P = .0167$ (post hoc, AVF with stenosis vs sham, day 21; n = 5-8).

mice with an AVF, both without or with a stenosis, showed increased IVC wall thickness in both upstream and downstream segments (Fig 2, *E, G* and *H*). There was no significant difference between wall thickness in mice with an AVF and with a stenosis compared with AVF without a stenosis (Fig 2, *E, G* and *H*). These data show that the presence of an AVF is associated with a thickened IVC wall, more prominently upstream of the stenosis, but still present downstream of the stenosis.

In the segments that exhibited prominent wall thickening, namely, upstream of the stenosis in mice with an AVF without or with a stenosis, we determined the cell and extracellular matrix composition. In mice with an AVF, both without and with a distal stenosis, the majority of cells in the intima-media of the IVC wall at day 21 were α-smooth muscle actin-positive, with no difference in cell density between the 2 groups (Supplementary Fig, *A* and *B*). CD68-positive cells and CD3-positive cells were observed primarily in the adventitia but not in the intima-media of the IVC wall, with no difference in quantity between the two groups (Supplementary Fig, *C* and *D*). Collagen was abundant in all layers of the IVC wall with no significant difference between the two groups (Supplementary Fig, *E* and *F*). These data suggest similar wall composition in the fistulae without and with a distal stenosis, at day 21.

AVF patency was assessed by confirmation of increased EDV in the aorta proximal to the fistula, and loss of increased EDV was considered AVF failure (Fig 1, *B*). In sham-operated mice, and mice with stenosis alone, there were no mice with AVF or venous occlusion (Fig 2, *I*; black and green); however, AVF patency significantly decreased in mice with an AVF with stenosis, compared with mice with an AVF alone (Fig 2, *I*; red vs blue). These data show that the presence of an IVC stenosis distal to the fistula decreases AVF patency.

The mortality rate of mice with both an AVF and a stenosis was 25% at day 3 and, although this rate

was higher than mice with an AVF but without a stenosis (10% at day 3), this difference was not statistically significant (Fig 2, *J*; red vs blue).

Physiologic properties of the mouse infrarenal aorta. To study the physiologic changes associated with an AVF without or with distal stenosis, mice were examined serially with ultrasound postoperatively. The infrarenal aorta, that is, the proximal inflow into the fistula, was examined for waveform, PSV, EDV, and blood flow, and the resistance index and shear stress were calculated (Fig 3; see also Fig 1, *B-D*). Sham-operated mice and those with a distal stenosis alone, without an AVF, showed similar Doppler measurements (Fig 3, *A-F*; black vs green). Thus, partial ligation of the IVC without an aortocaval fistula did not have a detectable effect on the aorta.

However, the addition of an AVF significantly increased PSV, EDV, blood flow, and shear stress, while decreasing the resistance index in the aorta, as compared with sham-operated mice (Fig 3, *A-F*; blue vs black). Further, addition of the IVC distal stenosis did not change any of these measurements in the aorta, compared with mice with an AVF alone (Fig 3, *A-F*; red vs blue). These data show that the presence of the fistula has a measurable effect on the aortic blood flow, that is, the proximal inflow into the fistula.

Physiologic properties of the mouse infrarenal IVC. Doppler measurements were also obtained in the IVC at 3 separate locations: at the stenosis, 2 mm upstream (caudal) to the stenosis, and 2 mm downstream (cranial) to the stenosis (Fig 1, *A*). Doppler waveforms of the IVC in the sham-operated mice showed consistent venous waveforms throughout the segments (Fig 4, *A*; first row). In mice with an AVF but without a stenosis, the venous waveforms gained pulsatility that became clearer downstream, that is, with increased prominence of the spectral window (Fig 4, *A*; second row, Fig 1, *C*). In addition, TAMV and spectral broadening were increased in all segments of the IVC compared with sham-operated mice (Fig 4, *B-C*; blue vs black).

In mice with an IVC stenosis alone, that is, without an AVF, the IVC waveforms showed similar properties compared with those of sham-operated mice, especially the waveform morphology (Fig 4, *A*; third row), TAMV (Fig 4, *B* and *D*; green vs black), and spectral broadening, both upstream and downstream of the stenosis (Fig 4, *E, G*; green vs black). However, mice with an IVC stenosis alone had increased TAMV and spectral broadening at the stenosis, as compared with sham-operated mice (Fig 4, *C* and *F*; green vs black).

In mice with both an IVC stenosis and an AVF, the waveforms showed pulsatility (Fig 4, *A*; fourth row) and increased TAMV (Fig 4, *B* and *C*; red vs blue), as well as increased spectral broadening (Fig 4, *E* and *F*; red vs blue), compared with mice with a fistula but without an IVC stenosis, both downstream and at the stenosis. There were no differences in TAMV and spectral broadening between these two groups upstream of the stenosis (Fig 4, *D, G*; red vs blue).

In the mice with an AVF, the amount of spectral broadening was also normalized to the maximum velocity, allowing quantification of the spectral window (Fig 1, *C*). In mice without an AVF, the venous waveforms had low velocities that prevented detection of the spectral window. Mice with an AVF but without a stenosis showed a decreased spectral broadening index compared with mice with both an AVF and a stenosis, both downstream and at the stenosis, but no difference was seen upstream of the stenosis (Fig 4, *H-J*). These data suggest that mice with an AVF but without a stenosis show return to laminar flow in the IVC distal to the AVF (at the downstream site), whereas mice with both an AVF and a stenosis show disturbed flow throughout the IVC.

Differential immunoreactivity of mechanosensitive proteins. Because our data suggest different frequencies of shear stress in the IVC of mice with an AVF and a stenosis, compared with those with an AVF but without a stenosis (Fig 4, *H*; red vs blue), we evaluated several proteins whose expression is regulated by shear stress. Although both Klf2 and p-eNOS showed no difference in immunoreactivity in the IVC endothelium upstream of the stenosis, between mice with an AVF and a stenosis compared with mice with an AVF and without a stenosis (Fig 5, *A* and *B*), there was a trend towards decreased immunoreactivity downstream of the stenosis (Fig 5, *C* and *D*) in matched samples. These data suggests that there is different shear stress in the IVC downstream of the stenosis, compared with the pattern present without a stenosis.

Changes in Doppler waveforms in a human case of percutaneous angioplasty. Because the mouse ultrasound data suggest that stenosis distal to an AVF shows disturbed flow, we examined a male human patient with CVS distal to a functional AVF (Fig 6, *A*), both before and after angioplasty to treat the stenosis, using a transducer-equipped guidewire to obtain the Doppler waveforms. Before angioplasty, the Doppler waveforms showed pulsatility and a prominent increase in velocity at the site of stenosis, as well as downstream to the stenosis (Fig 6, *B*; top row). These waveforms diminished after angioplasty, consistent with angiographic resolution of the stenosis (Fig 6, *B*; bottom row). These demonstrative human waveforms suggest that the data obtained from the mouse model may be a faithful representation of human waveforms, at least in some instances.

DISCUSSION

This study describes a novel mouse model of stenosis distal to an AVF that displays wall thickening and decreased vessel diameter downstream of the stenosis,

resulting in significantly worse AVF patency (Fig 2). A lack of transition to laminar shear stress distal to the stenosis (Figs 4 and 5), with continued disturbed shear stress (Fig 4), suggests a mechanism for the decreased AVF patency, with similar Doppler waveforms to those observed in a case of a human patient with CVS distal to an AVF (Fig 6). These data suggest that this mouse model of stenosis distal to an AVF may recapitulate the pathophysiology of human CVS.

The gold standard of access surveillance in patients on hemodialysis is Doppler ultrasound examination, although its usefulness is limited to fully visualize proximal central veins.[19] As such, even though disturbed flow can be seen downstream to CVS using venography,[20] quantitative analyses of the disturbance are not well-described. In our human case that used percutaneous angioplasty to treat CVS distal to a functional AVF, a transducer-equipped guidewire was used to show Doppler waveforms that are comparable with those seen in the mouse model (Fig 6). Because transducer-equipped guidewires are not commonly used, our highly valuable data show the translational relevance of the mouse model and suggest the importance of shear stress in the pathophysiology of human CVS. Interestingly, the postangioplasty human waveforms show partial but not complete resolution of the downstream pulsatility despite angiographic resolution of the stenosis (Fig 6, *B*), suggesting that postprocedure venography may be inadequate to assess low degrees of residual stenosis. Future treatment of human CVS may require other modalities of assessment, such as transducer-equipped guidewires. Magnetic resonance imaging is capable of assessing lumen geometry and flow volume measurements without the need of contrast and correlates with Doppler ultrasound studies of human AVF.[21,22] However, magnetic resonance imaging is time consuming and expensive, and not currently practical for routine assessment of CVS.

This model shows that the Doppler waveforms in the IVC distal to an AVF show disturbed waveforms throughout the IVC in mice with a stenosis, whereas mice with an AVF but without a stenosis show laminar waveforms downstream of the stenosis (Fig 4). The loss of the spectral window, that is, increased spectral broadening, is consistent with disturbed shear stress.[14,15] Because the absolute value of spectral broadening depends on the maximum velocity, we used the spectral broadening index, which normalizes spectral broadening to the maximum velocity, to measure disturbed flow. Originally, the spectral broadening index was validated with an in vitro flow model,[14] and the index efficiently quantifies the severity of flow disturbances that are present distal to a stenosis, using data acquired from human carotid arteries.[14,15] Here, the spectral broadening index was able to discriminate between the patterns without and with a stenosis distal to an AVF. Mice without a distal stenosis showed a decrease in the index moving from upstream to downstream, consistent with restoration of the spectral window (Fig 4, *H-J*, blue line), whereas mice with a distal stenosis retained high values of the index consistent with lack of the spectral window (Fig 4, *H-J*, red line). In human patients where Doppler ultrasound waveforms are obtainable, the spectral broadening index may be useful to detect flow disturbance without visual confirmation of the stenosis itself.

We were not able to calculate shear stress in the IVC distal to an AVF using the velocity of the blood flow and the vessel diameter for two important reasons. First, the Hagen-Poiseuille equation that is used to calculate shear stress in the aorta assumes laminar blood flow.[23] In this model, venous Doppler waveforms in mice having both an AVF and a stenosis are consistent with disturbed waveforms; similarly, in mice with an AVF but without a stenosis, disturbed waveforms were prominent adjacent to the fistula (Fig 4). Second is the limitation of the gate size of ultrasound probes in the pulse wave mode. Because the diameter of the IVC after AVF creation exceeds the maximum sample volume of the probe, the TAMV may be overestimated owing to the loss of low-velocity components near the vessel wall.

Because we could not quantify the shear stress in the IVC based on ultrasound measurements, we used a molecular approach to confirm decreased laminar shear stress downstream of a distal stenosis (Fig 5). Klf-2 is a zinc finger-containing transcription factor abundantly expressed in the endothelium[24] and is associated with atheroprotection by inhibiting inflammation and thrombosis, as well as stimulating vasodilation by upregulating eNOS.[25,26] Klf-2 expression is upregulated by laminar shear stress and downregulated by disturbed shear stress.[11,24] Our data show a trend toward decreased immunoreactivity of both Klf-2 and p-eNOS downstream (Fig 5 *C* and *D*) but not upstream (Fig 5, *A* and *B*) of a distal stenosis, compatible with our ultrasound findings showing diminished laminar shear stress in this exact region (Fig 4). This finding is also compatible with a previous study showing diminished Klf-2 expression in the endothelium at the poststenotic site in a rat aortic stenosis model.[24] As expected of all animal models,[27,28] our mouse model does not perfectly recapitulate all aspects of the molecular and cellular responses that occur during formation of a stenosis, because our partial ligation of the IVC is an acute model; however, we believe that our model enables study the physiologic and molecular changes after the formation of an established stenosis that has disturbed flow.

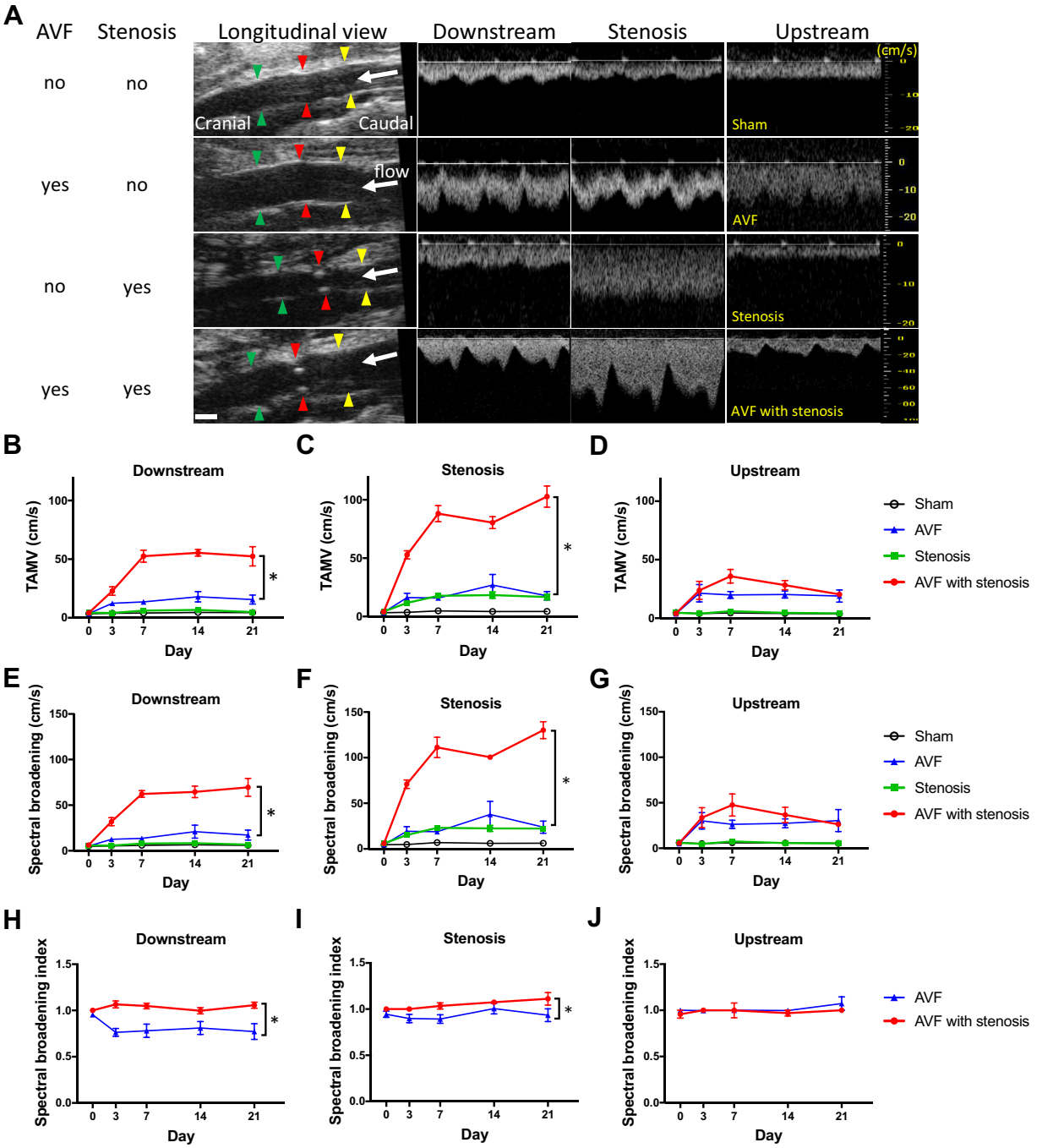

Fig 4. Physiologic properties of the mouse inferior vena cava (IVC). **A,** Representative Doppler waveforms of the IVC at postoperative day 3. In the longitudinal view (left most column), red arrowheads indicate the stenosis; yellow arrowheads indicate site of insonation 2 mm upstream; green arrowhead indicates site of insonation 2 mm downstream of the stenosis. Scale bar = 1 mm. **B-D,** Line graph showing time-averaged maximum velocity (*TAMV*) of the IVC **(B)** downstream ($P < .0001$; analysis of variance [ANOVA]). *$P < .0001$ (post hoc, arteriovenous fistula [*AVF*] with stenosis vs AVF at day 21). **C,** Stenosis ($P < .0001$, ANOVA). *$P < .0001$ (post hoc, AVF with stenosis vs AVF at day 21). **D,** Upstream ($P < .0001$, ANOVA; $P = .9887$, post hoc; AVF with stenosis vs AVF at day 21; n = 4-8). **E-G,** Line graph showing spectral broadening of the IVC **(E)** downstream ($P < .0001$, ANOVA). *$P < .0001$ (post hoc, AVF with stenosis vs AVF at day 21). **F,** Stenosis ($P < .0001$, ANOVA). *$P < .0001$ (post hoc, AVF with stenosis vs AVF at day 21). **G,** Upstream ($P < .0001$, ANOVA; $P = .9412$, post hoc; AVF with stenosis vs AVF at day 21; n = 4-8). **H-J,** Line graph showing spectral broadening index of the IVC in mice with AVF **(H)** downstream ($P < .0052$, ANOVA). *$P = .0108$ (post hoc, AVF with stenosis vs AVF at day 21). **I,** Stenosis ($P = .0224$, ANOVA). *$P = .0588$ (post hoc, AVF with stenosis vs AVF at day 21). **J,** Upstream ($P = .3219$, ANOVA; n = 4-8).

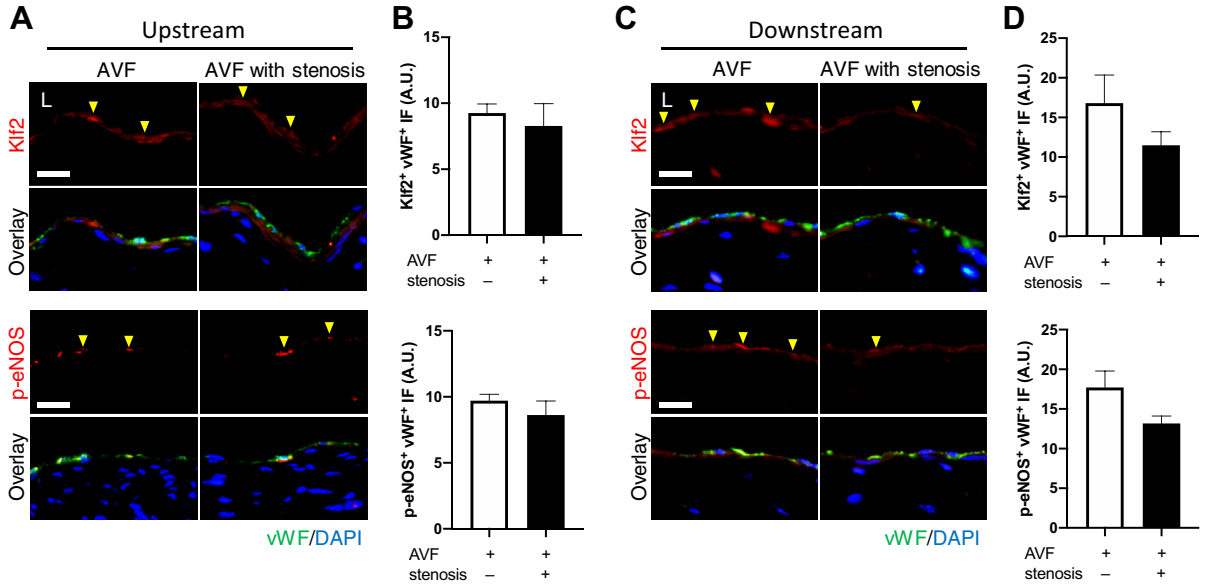

Fig 5. Expression of mechanosensitive proteins in the mouse inferior vena cava (IVC). **A,** Representative immunofluorescence photomicrographs of IVC sections at day 21 with anti-von Willebrand factor (*vWF*), anti-Krüppel-like factor 2 (*Klf2*) (upper panels), and anti-phosphorylated endothelial nitric oxide synthase (*p-eNOS*) (lower panels) antibodies in arteriovenous fistula (*AVF*) vs AVF with stenosis, upstream of stenosis. Scale bar = 20 μm. **B,** Bar graphs showing quantification of Klf2 (top) and p-eNOS (bottom) positive signal in the endothelium, upstream; Klf2 vWF: $P = .6102$ (*t*-test), p-eNOS vWF: $P = .3843$ (*t*-test); n = 4. **C,** Representative immunofluorescence photomicrographs of IVC sections at day 21 with anti-vWF, anti-Klf2 (upper panels) and anti-p-eNOS (lower panels) antibodies in AVF vs AVF with stenosis, downstream of stenosis. Scale bar = 20 μm. **D,** Bar graphs showing quantification of Klf2 (top) and p-eNOS (bottom) positive signal in the endothelium, downstream; vWF Klf2: $P = .2243$ (*t*-test), vWF p-eNOS: $P = .0905$ (*t*-test); n = 4. *L*, Lumen.

Partial IVC ligation was used to create the stenosis and modified from the method to create a mouse model of deep venous thrombosis.[29-31] Previous studies showed that complete ligation of the IVC generates a venous stasis model with thrombus formation in 80% to 90% of the mice.[29,31] In a more severe stenosis model, using a spacer with less than one-half the diameter than we used, a high incidence of thrombosis was observed.[29,30] Here, we used a 22-G catheter to generate a lesser degree of stenosis, in which we observed no thrombus formation (Fig 2, *I*). Of note, the placement of the IVC ligation in our model was positioned upstream (caudal) to the consistent iliolumbar veins because we wanted to minimize the potential for these veins to serve as collaterals if the stenosis was placed downstream (cranial) from these veins (Fig 1, *A*); accordingly, we did not observe any prominent collaterals around the stenosis at the time of tissue collection.

Another benefit of this technique is its high reproducibility; regardless of whether an AVF was present or not, the diameter at the site of stenosis was consistently 0.6 mm up to day 21 as measured by Doppler ultrasound examination, and as expected from the presence of an intact ligature (Fig 2, *C*). We have previously shown that this technique will create a 40% stenosis in mice with a stenosis but without an AVF and a 60% stenosis in mice with both a stenosis and an AVF.[9] Because the waveforms in this model are remarkably similar to waveforms observed in a case of human CVS (Fig 6), we believe that this reproducible animal model potentially allows observation of data that is translationally relevant to human CVS. For example, this model shows reduced patency compared with AVF without stenosis. In the mouse AVF model without a distal stenosis, approximately 10% of AVF occlude by day 3 (Fig 2, *I*; blue) owing to technical issues most frequently secondary to excessive pressure on the fistula while achieving hemostasis.[8] In contrast, 40% of mice with both an AVF and a stenosis occlude by day 3 and 50% are occluded by day 7 (Fig 2, *I*; red); these data suggest that AVF with distal stenosis have decreased patency secondary to the stenosis, that is, secondary to the disease beyond the immediate technical loss of patency.

One of the limitations of this study is the exclusive use of male animals. Studies with female mice are important because female sex is an important variable that predicts reduced maturation in human AVF.[32,33] In this mouse AVF model, female mice show diminished AVF patency preceded by reduced magnitudes of laminar shear stress.[13] Additional studies in female mice with distal stenosis are now warranted. Improvement of the maximum gate length of ultrasound probes may also help to visualize the entire spectrum of the flow velocity in the dilated vein. Another limitation of our CVS model is the

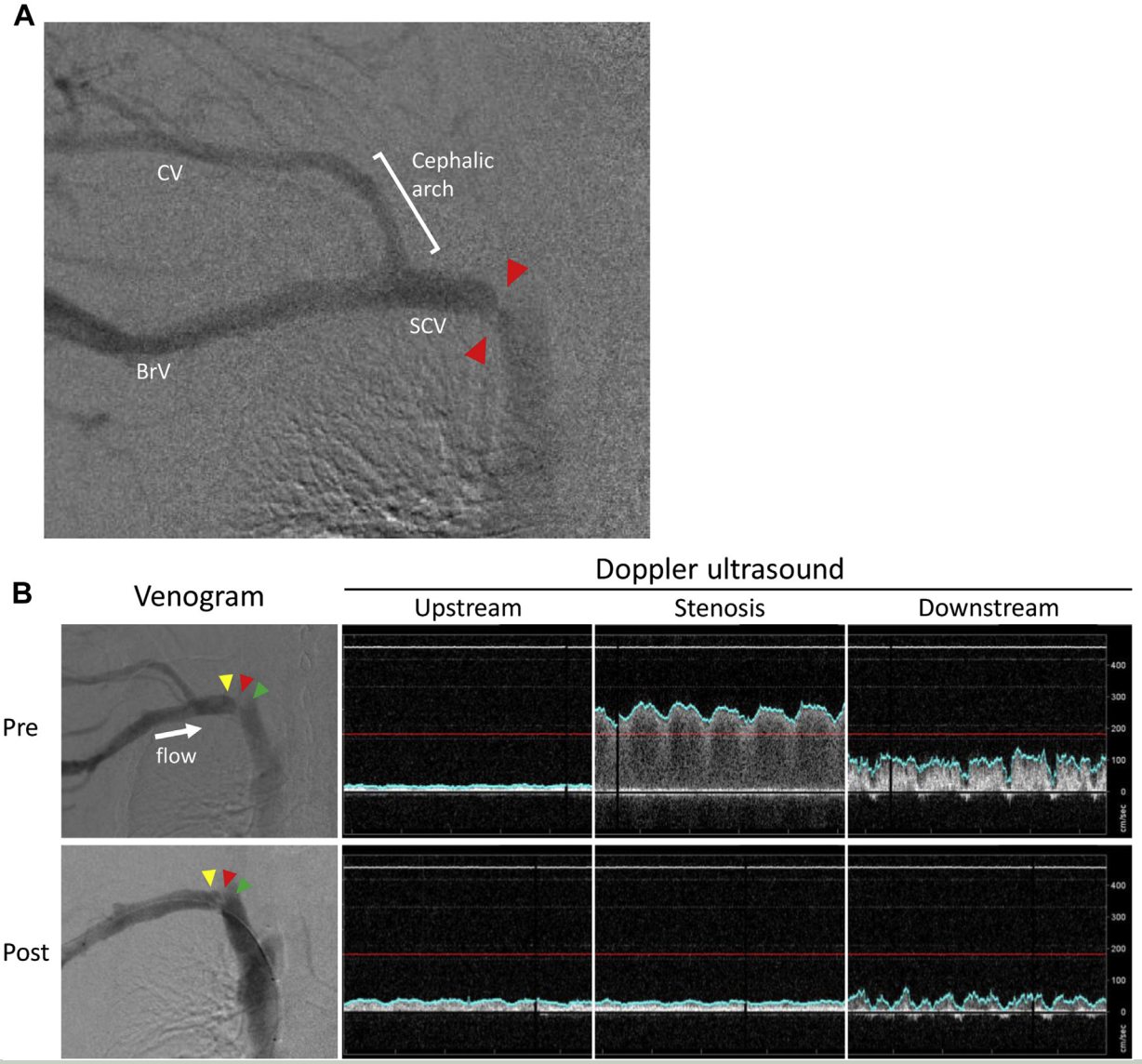

Fig 6. Central stenosis in the outflow of an arteriovenous fistula (AVF) in a human case. **A,** Venogram showing central venous stenosis (CVS) in a human patient. A severe stenosis is visible in the proximal right subclavian vein (*red arrowhead*). **B,** Venogram (left column) and Doppler waveforms (right columns) before (top row) and after (bottom row) percutaneous angioplasty of the stenosis in the same case. Doppler waveforms were obtained at the stenosis (*red arrowhead*) as well as upstream (*yellow arrowhead*) and downstream (*green arrowhead*) to the stenosis. *BrV,* Brachial vein; *CV,* cephalic vein; *SCV,* subclavian vein.

potential inflammatory effects of vessel exposure or the mechanical compression of the suture since these factors are known to promote intimal hyperplasia and may contribute to differences in vascular remodeling within our experimental groups.[34] In addition, because the stenosis in this model is a very short segment, examination of different lengths and degrees of stenosis may allow greater modeling of different ranges of human CVS. Last, the limited number of human subjects in this study requires future studies with a substantial number of human patients to strengthen the validity of this mouse model.

CONCLUSIONS

Our mouse model of stenosis distal to an AVF shows disturbed shear stress and decreased laminar shear stress, with significantly reduced fistula patency; the waveforms are comparable to those in a human case of CVS. A further understanding of the pathophysiology and downstream molecular signaling of this novel mouse model may help us to understand the mechanisms of AVF failure caused by human CVS.

This work was supported by US National Institute of Health (NIH) grants R01-HL128406 and R01-HL144476 [to

A.D.]; the United States Department of Veterans Affairs Biomedical Laboratory Research and Development Program Merit Review Award I01-BX002336 [to A.D.]; an Uehara Memorial Foundation postdoctoral fellowship [to Y.M.]; as well as with the resources and the use of facilities at the VA Connecticut Healthcare System, West Haven, Connecticut.

AUTHOR CONTRIBUTIONS

Conception and design: RT, SO, TI, JK, TN, KH, AD
Analysis and interpretation: RT, SO, JG, SL, YM, BY
Data collection: RT, SO, TI
Writing the article: RT
Critical revision of the article: SO, TI, JG, SL, YM, BY, JK, TN, KH, AD
Final approval of the article: RT, SO, TI, JG, SL, YM, BY, JK, TN, KH, AD
Statistical analysis: RT
Obtained funding: AD
Overall responsibility: AD
RT and SO contributed equally to this article and share co-first authorship.

REFERENCES

1. Saran R, Robinson B, Abbott KC, Bragg-Gresham J, Chen X, Gipson D, et al. US Renal Data System 2019 Annual Data Report: epidemiology of kidney disease in the United States. Am J Kidney Dis 2020;75:A6-7.
2. Almasri J, Alsawas M, Mainou M, Mustafa RA, Wang Z, Woo K, et al. Outcomes of vascular access for hemodialysis: a systematic review and meta-analysis. J Vasc Surg 2016;64:236-43.
3. Murad MH, Elamin MB, Sidawy AN, Malaga G, Rizvi AZ, Flynn DN, et al. Autogenous versus prosthetic vascular access for hemodialysis: a systematic review and meta-analysis. J Vasc Surg 2008;48:34S-47S.
4. Donca IZ, Wish JB. Systemic barriers to optimal hemodialysis access. Semin Nephrol 2012;32:519-29.
5. Huijbregts HJ, Bots ML, Wittens CH, Schrama YC, Moll FL, Blankestijn PJ, et al. Hemodialysis arteriovenous fistula patency revisited: results of a prospective, multicenter initiative. Clin J Am Soc Nephrol 2008;3:714-9.
6. Quencer KB, Arici M. Arteriovenous fistulas and their characteristic sites of stenosis. AJR Am J Roentgenol 2015;205:726-34.
7. Roy-Chaudhury P, Sukhatme VP, Cheung AK. Hemodialysis vascular access dysfunction: a cellular and molecular viewpoint. J Am Soc Nephrol 2006;17:1112-27.
8. Yamamoto K, Protack CD, Tsuneki M, Hall MR, Wong DJ, Lu DY, et al. The mouse aortocaval fistula recapitulates human arteriovenous fistula maturation. Am J Physiol Heart Circ Physiol 2013;305:H1718-25.
9. Isaji T, Ono S, Hashimoto T, Yamamoto K, Taniguchi R, Hu H, et al. Murine model of central venous stenosis using aortocaval fistula with an outflow stenosis. J Vis Exp 2019 Jul 11. [Epub ahead of print].
10. Yamamoto K, Protack CD, Kuwahara G, Tsuneki M, Hashimoto T, Hall MR, et al. Disturbed shear stress reduces Klf2 expression in arterial-venous fistulae in vivo. Physiol Rep 2015;3.
11. Chiu JJ, Chien S. Effects of disturbed flow on vascular endothelium: pathophysiological basis and clinical perspectives. Physiol Rev 2011;91:327-87.
12. Topper JN, Gimbrone MA. Blood flow and vascular gene expression: fluid shear stress as a modulator of endothelial phenotype. Mol Med Today 1999;5:40-6.
13. Kudze T, Ono S, Fereydooni A, Gonzalez L, Isaji T, Hu H, et al. Altered hemodynamics during arteriovenous fistula remodeling leads to reduced fistula patency in female mice. JVS-Vasc Sci 2020;1:42-56.
14. Kassam M, Johnston KW, Cobbold RS. Quantitative estimation of spectral broadening for the diagnosis of carotid arterial disease: method and in vitro results. Ultrasound Med Biol 1985;11:425-33.
15. Johnston KW, Baker WH, Burnham SJ, Hayes AC, Kupper CA, Poole MA. Quantitative analysis of continuous-wave Doppler spectral broadening for the diagnosis of carotid disease: results of a multicenter study. J Vasc Surg 1986;4:493-504.
16. Bulley S, Fernández-Peña C, Hasan R, Leo MD, Muralidharan P, Mackay CE, et al. Arterial smooth muscle cell PKD2 (TRPP1) channels regulate systemic blood pressure. Elife 2018;7.
17. Hashimoto T, Isaji T, Hu H, Yamamoto K, Bai H, Santana JM, et al. Stimulation of caveolin-1 signaling improves arteriovenous fistula patency. Arterioscler Thromb Vasc Biol 2019;39:754-64.
18. Guo X, Fereydooni A, Isaji T, Gorecka J, Liu S, Hu H, et al. Inhibition of the Akt1-mTORC1 axis alters venous remodeling to improve arteriovenous fistula patency. Sci Rep 2019;9:11046.
19. Vascular Accsess Work Group. Clinical practice guidelines for vascular access. Am J Kidney Dis 2006;48(Suppl 1):S248-73.
20. Agarwal AK. Central vein stenosis. Am J Kidney Dis 2013;61:1001-15.
21. He Y, Terry CM, Nguyen C, Berceli SA, Shiu YT, Cheung AK. Serial analysis of lumen geometry and hemodynamics in human arteriovenous fistula for hemodialysis using magnetic resonance imaging and computational fluid dynamics. J Biomech 2013;46:165-9.
22. He Y, Shiu YT, Pike DB, Roy-Chaudhury P, Cheung AK, Berceli SA. Comparison of hemodialysis arteriovenous fistula blood flow rates measured by Doppler ultrasound and phase-contrast magnetic resonance imaging. J Vasc Surg 2018;68:1848-57.e2.
23. Sutera SP, Skalak R. The history of Poiseuille's law. Annu Rev Fluid Mech 1993;25:1-20.
24. Wang N, Miao H, Li YS, Zhang P, Haga JH, Hu Y, et al. Shear stress regulation of Krüppel-like factor 2 expression is flow pattern-specific. Biochem Biophys Res Commun 2006;341:1244-51.
25. Fledderus JO, van Thienen JV, Boon RA, Dekker RJ, Rohlena J, Volger OL, et al. Prolonged shear stress and KLF2 suppress constitutive proinflammatory transcription through inhibition of ATF2. Blood 2007;109:4249-57.
26. Novodvorsky P, Chico TJ. The role of the transcription factor KLF2 in vascular development and disease. Prog Mol Biol Transl Sci 2014;124:155-88.
27. Hartung T. Thoughts on limitations of animal models. Parkinsonism Relat Disord 2008;14(Suppl 2):S81-3.
28. Rotmans JI. Animal models for studying pathophysiology of hemodialysis access. Open Urol Nephrol J 2014;7:14-21.
29. Brill A, Fuchs TA, Chauhan AK, Yang JJ, De Meyer SF, Köllnberger M, et al. von Willebrand factor-mediated platelet adhesion is critical for deep vein thrombosis in mouse models. Blood 2011;117:1400-7.
30. von Brühl ML, Stark K, Steinhart A, Chandraratne S, Konrad I, Lorenz M, et al. Monocytes, neutrophils, and platelets

cooperate to initiate and propagate venous thrombosis in mice in vivo. J Exp Med 2012;209:819-35.
31. Myers DD, Hawley AE, Farris DM, Wrobleski SK, Thanaporn P, Schaub RG, et al. P-selectin and leukocyte microparticles are associated with venous thrombogenesis. J Vasc Surg 2003;38:1075-89.
32. Miller CD, Robbin ML, Allon M. Gender differences in outcomes of arteriovenous fistulas in hemodialysis patients. Kidney Int 2003;63:346-52.
33. Peterson WJ, Barker J, Allon M. Disparities in fistula maturation persist despite preoperative vascular mapping. Clin J Am Soc Nephrol 2008;3:437-41.
34. Clowes AW. Chapter 17 Intimal hyperplasia and graft failure. Cardiovasc Pathol 1993;2:179-86.

Submitted Mar 23, 2020; accepted Jul 9, 2020.

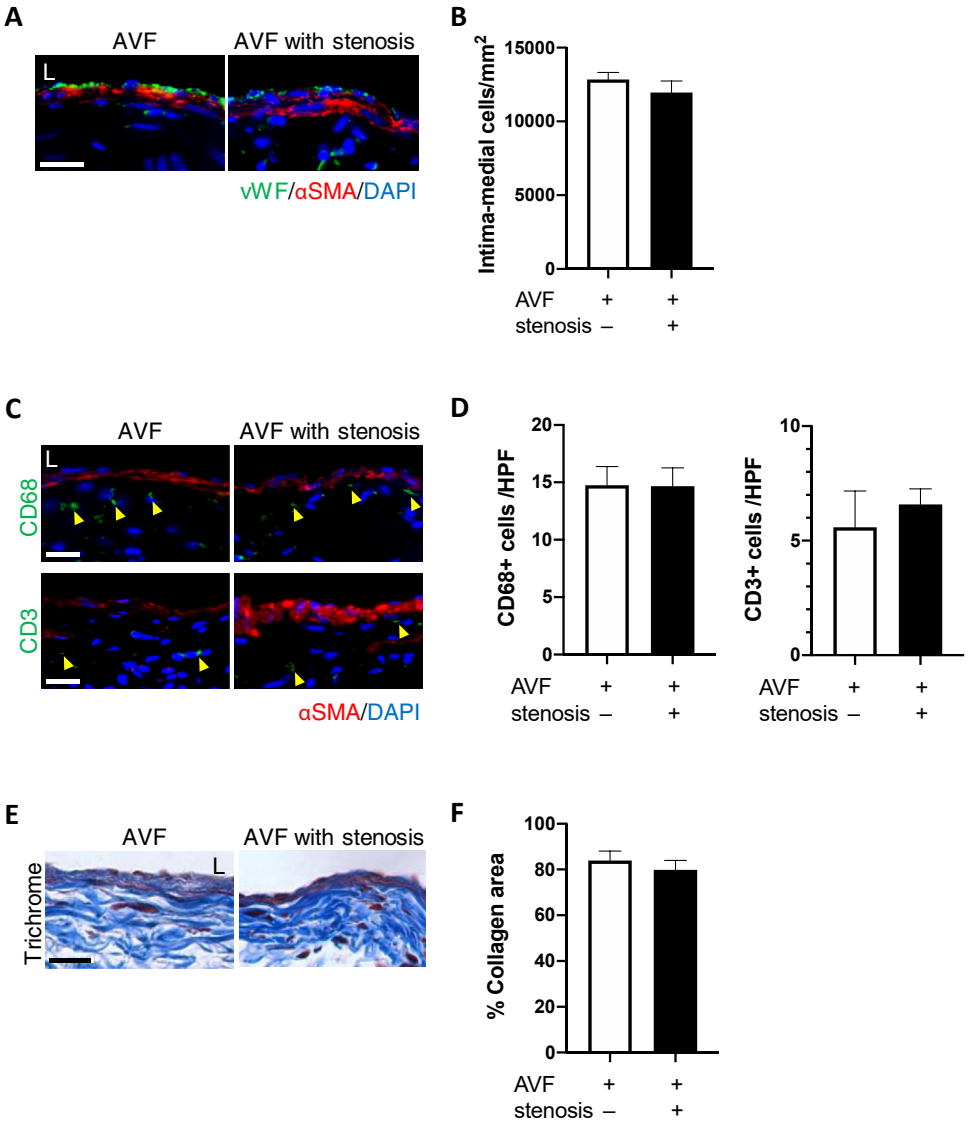

Supplementary Fig. Fistula wall composition at postoperative day 21. **A,** Representative immunofluorescence (IF) photomicrographs of inferior vena cava (IVC) at day 21 with anti-von Willebrand factor (*vWF*) and anti-α-smooth muscle actin (*α-SMA*) antibodies, upstream of the stenosis. Scale bar = 20 μm. **B,** Bar graphs showing number of cells in the intima and media per area; $P = .3951$ (*t*-test); n = 3. **C,** Representative IF photomicrographs of IVC at day 21 with anti-CD68 (top row) or anti-CD3 (*bottom row*) and anti-α-SMA antibodies, upstream of the stenosis. Scale bar = 20 μm. **D,** Bar graphs showing number of $CD68^+$ or $CD3^+$ cells in the IVC wall; CD68; $P = .9725$; CD3; $P = .5942$ (*t*-test); n = 3. (E) Representative photomicrographs of Masson's trichrome staining of the IVC, upstream of the stenosis, at day 21. Scale bar = 20 μm. **F,** Bar graphs showing % collagen area in the IVC wall; $P = .4986$; n = 4. *AVF,* Arteriovenous fistula; *HPF,* high-power field; *L,* lumen.